Nanochem Res 9(2): 77-90, Spring 2024

RESEARCH PAPER

Antibacterial, Antifungal and Cytotoxic Properties as well as Molecular Docking Evaluation of Green Synthesized Silver Nanoparticles

Mojgan Taebi[1], Mahnaz Amiri[2,*], Niloofar Rashidi[1], Mahsa Ziasistani[3], Sanaz Hadizadeh[4], Razieh Razavi[5,*], Alireza Farsinejad[6], Meysam Ahmadi Zeidabadi[2], Somayyeh Karami-mohajeri[7]

[1] Department of Anesthesia,Faculty of Allied Medical Sciences,Kerman University of Medical Sciences,Kerman,Iran

[2] Neuroscience Research Center, Institute of Neuropharmacology, Kerman University of Medical Science, Kerman, Iran

[3] Pathology and Stem Cell Research Center, Afzalipour Hospital, Kerman University of Medical Science, Kerman, Iran

[4] Department of Medical Mycology & Parasitology, Faculty of Medicine, Kerman University of Medical Sciences, Kerman, Iran

[5] Department of chemistry, Faculty of Science, University of Jiroft, Jiroft, Iran

[6] Department of Laboratory Hematology and Blood Banking, Faculty of Allied Medicine, Kerman University of Medical Sciences, Kerman, Iran

[7] Department of Toxicology and Pharmacology, School of PharmacyKerman University of Medical Sciences, Kerman, Iran

ARTICLE INFO

Article History:
Received 07 January 2024
Accepted 25 February 2024
Published 15 April 2024

Keywords:
Silver nanoparticle
Green synthesis
Antifungal effect
Antibacterial activity
Cytotoxicity
Herbal extract
Molecular docking

ABSTRACT

The utilization of silver nanoparticles (AgNPs) in diverse fields, including medicine, is on the rise, leading to the development of a non-toxic and environmentally friendly synthesis method. This study presents a straightforward and stable one-step synthesis of AgNPs using an aqueous extract of Amygdalus lycioides as both a reducing and stabilizing agent. The experimental findings demonstrated that the presence of Amygdalus lycioides extract results in the formation of AgNPs with smaller size, uniformity, and well-dispersed nanostructures. The synthesis process is significantly influenced by certain reaction parameters such as the molar ratio of $AgNO_3$, temperature, and extract volume. Characterization of the nanostructures was performed using XRD, UV-Vis, FT-IR, DLS, and SEM measurements. Furthermore, the AgNPs exhibited potent antibacterial effects, leading to cell death through increasing the membrane permeability and disrupting bacterial wall integrity. Additionally, this research explores the fungicidal characteristics of the colloidal solution of nanosized silver as a potential antifungal treatment against various plant pathogens. Based on the obtained results, AgNPs exhibit varying levels of antifungal activity against these plant pathogens. Molecular docking calculations revealed the binding energy between Ag metal and bacteria. These findings pave the way for effective and novel antimicrobial therapies as alternatives to traditional antifungal and antibacterial drugs, thereby addressing the challenges of microbial resistance and the difficulty of eradicating infections in the near future.

How to cite this article
Taebi M., Amiri M., Rashidi N., Ziasistani M., Hadizadeh S., Razavi R., Farsinejad A., Ahmadi Zeidabadi M., Karami-mohajeri S. Antibacterial, Antifungal and Cytotoxic Properties as well as Molecular Docking Evaluation of Green Synthesized Silver Nanoparticles . Nanochem Res, 2024; 9(2):77-90. DOI: 10.22036/ncr.2024.02.001

* Corresponding Author Email: *r.razavi@ujiroft.ac.ir*
ma.amiri@kmu.ac.ir

INTRODUCTION

At present, nanotechnology is recognized as a progressive scientific domain that encompasses a wide range of nanoparticles varying in size, shape, and chemical composition, offering various potential applications [1]. Extensive literature has documented numerous methods for the synthesis of nanoparticles using precious heavy metals like Pt, Pd, Ag, and Au [2,3]. Silver nanoparticles (AgNPs) play a significant role among noble metal nanoparticles due to their distinctive structural characteristics and properties in plasmonics and physical chemistry. These properties include surface functionalization and controlled drug release, making them highly versatile [4].

AgNPs are particularly effective in antimicrobial applications due to their thermal stability, large surface area for Ag+ ion storage, and controlled release rate. The antimicrobial efficacy of AgNPs is influenced by factors such as geometric shape, size, and type of silver nanoparticles, as well as the synthesis methods employed [5]. Phenoxyethanol and paraben, commonly used as preservatives in cosmetics, have a temporary effect on skin condition and can increase sensitivity to ultraviolet (UV) light [6]. Silver and silver complexes have been utilized to control bacterial growth in different studies [7]. Various methods [8], such as chemical reduction [9], microwave irradiation [10], photoreduction [11], and thermal decomposition [12] have been reported for nanoparticle synthesis and design. However, these processes are often energy-intensive, expensive, and have potential negative impacts on the human health and environment. Therefore, there is a need to establish environmentally friendly alternatives [13]. Green synthesis refers to the advancement of physical and chemical processes that are environmentally friendly, cost-effective, and can be easily scaled up for large-scale synthesis without the need for high pressure, excessive temperature, energy consumption, or toxic substances. In this approach, enzymes, plant extracts, and microorganisms are utilized to bioreduce metal ions and form chemical complexes [14] in a highly efficient manner. Among various green synthesis methods, the utilization of plants for nanoparticle synthesis has emerged as a promising approach. This plant-mediated synthesis offers several advantages, including shorter synthesis times and improved stability of the resulting nanoparticles [15]. Consequently, there has been significant interest in developing methodologies for effectively controlling the size of nanoparticles using this bio-inspired approach [16]. The biomolecules found in plants have demonstrated a significant role in the formation of nanoparticles, resulting in the production of nanoparticles with diverse sizes and shapes. This phenomenon has contributed to the advancement of eco-friendly methods in nanoparticle synthesis [17]. A variety of biomolecules present in plants have been identified to act as both capping and reducing agents during the synthesis of nanoparticles [18]. Many plants possess natural biosurfactant molecules that exhibit excellent foaming, wetting, and oil dispersion properties. These molecules consist of nonionic triterpenoid glycosides, which form the hydrophobic portion, and sugars, which make up the hydrophilic portion of the biosurfactant [19]. Different parts of plants, such as flowers, bark, leaves, fruits, and seeds, have been utilized for the synthesis of nanoparticles [20]. Recent studies have demonstrated the plant-mediated synthesis of silver nanoparticles using floral extracts of Calotropis procera, Hibiscus rosa-sinensis, and Delonix elata [21-23].

Silver nanoparticles (AgNPs) have been extensively utilized in medical materials as fillings and as antimicrobial agents due to their proven biocompatibility with mouse fibroblasts and human osteoblasts [24]. AgNPs exhibit low toxicity to human cells, high thermal stability, and low volatility. They are known for their strong biocidal properties, either by binding to the microbial cell wall and increasing membrane permeability or by inhibiting enzyme activity [25].

In this study, we present an innovative green synthesis method for the production of silver nanoparticles (AgNPs) using an aqueous herbal extract. The structure, morphology, and particle size of the synthesized nanoparticles were analyzed using several spectroscopic techniques. This study explores the previously unreported nanobiotechnological potential of the extract for AgNPs synthesis. Furthermore, the antibacterial, antifungal and cytotoxicity properties of the synthesized nanoparticles were investigated. Molecular docking analysis also supported the findings of this study.

EXPERIMENTAL

Materials and methods

The study utilized chemical materials of analytical purity, eliminating the need for further purification. Silver nitrate ($AgNO_3$, 99%) was acquired from Merck Company (Pvt. Ltd.) in

Germany. Various reagents and standard laboratory chemicals, including penicillin-streptomycin (100 µg/ml), Dulbecco's modified eagle's medium, fetal bovine serum (FBS), phosphate-buffered saline (PBS), trypsin-EDTA solution, dimethyl sulfoxide, trypan blue dye solution, iodonitrotetrazolium (INT), and Ciprofloxacin, were obtained from Sigma-Aldrich Company in the USA. The WST-1 reagent (2-(2-methoxy-4-nitrophenyl)-3-(4-nitrophenyl)-5-(2,4-disulfophenyl)-2H-tetrazolium) was prepared from Roche Holding AG. All eukaryote cells used in the study were sourced from the Pasteur Institute of Iran. Other materials employed in the research were provided as a gift by Arshanzist Youtab company in Iran.

Preparation of Lantana Amygdalus lycioides extract

The roots of Amygdalus lycioides were gathered from a forest in Kerman, Iran. The freshly collected roots were thoroughly washed three times and subsequently dried at a temperature of 25 °C. After drying, the roots were mechanically pulverized, sieved, and immersed in a mixture of distilled water and ethanol for a duration of three days. The resulting solution has been concentrated at 40 °C under reduced pressure by a rotary flash evaporator. Following this, the product was dried in an oven set at 60 °C, and the resulting extract was stored at a temperature of 4 °C.

Green synthesis procedures for silver nanoparticles

The green synthesis of silver nanoparticles involved the gradual addition of the extract to a separate solution of $AgNO_3$ while stirring at a speed of 500 rpm. The color of the reaction solutions quickly turned to light brown and became turbid. The solutions were left standing overnight, resulting in a dark brown color. The silver particles were then collected through centrifugation, washed three times with deionized water, and eventually dried at 40 °C in a vacuum oven.

To optimize the synthesis parameters of AgNPs, the effects of various factors were examined, including different concentrations of AgNO3 (ranging from 0.75 mM to 1.75 mM), varying volumes of the extract (1 to 5 mL), temperatures (27, 40, 60, 80 °C), and pH levels (8, 10, 12) in the presence of different extracts.

Microbial culture and antimicrobial activity of AgNPs

To assess the antimicrobial effect of the synthesized nanostructures, careful selection of microbial cultures was made, including M. luteus (ATCC 4698), B. subtilis (ATCC 6051), E. coli (ATCC 25922), S. aureus (ATCC 29213), K. pneumoniae (ATCC 13883), P. mirabilis (ATCC 21100), and P. aeruginosa (ATCC 27853).

Fresh cultures of these microbial strains were prepared using Mueller-Hinton agar and incubated overnight at 37 °C. A modified micro-dilution assay protocol was employed to evaluate the antibacterial effect [26]. The AgNPs were serially diluted (0.3–1000 µg/ml) in a 96-well round-bottom microplate.

Next, the microbial strains were cultured and incubated at 37 °C for 24 hours in the respective wells. After 24 hours, 40 µl of INT solution (0.6 mg/ml) was added to each well and incubated for 20 minutes at 37 °C. The absorbance of each solution was measured at 490 nm.

Ciprofloxacin was used as a positive control at concentrations ranging from 0.5 to 8 µg/ml, and a blank sample containing all reagents except the bacteria was included. The mortality rate percentage was calculated according to the following equation:

Mortality rate (%) = ((A-C) / (B-C)) × 100

where A represents the test sample; B denotes the positive control, and C stands for the negative control [27].

Antifungal activity assessment of AgNPs

To evaluate the antifungal properties of silver nanoparticles (AgNPs), the agar disc diffusion method was utilized with potato dextrose agar as the growth medium. Candida albicans, a test fungus, was chosen for the experiment. Inoculum preparation involved suspending colonies from 24-hour plate cultures in a 0.85% saline solution. The suspension's turbidity was matched to the 0.5 McFarland standards, resulting in a concentration of 1x106 CFU/ml.

A sterile cotton swab was saturated with the fungal suspension, and excess inoculum was removed by rotating the swab and pressing it against the tube's inner wall. The dried surface of a potato dextrose agar plate was streaked with the swab, ensuring complete coverage of the sterile agar surface. Agar discs loaded with silver nanoparticles were then placed on the inoculated plates, followed by incubation. The antifungal activity was determined by measuring the diameter of the zone of inhibition around the discs. A larger zone indicated stronger antifungal activity, with a minimum inhibitory concentration (MIC) of 500.

In order to ascertain the Minimum Fungicidal

Concentration (MFC), which represents the lowest concentration of nanoparticles needed to impact the viability of C. albicans, various concentrations of nanoparticles (ranging from 62.5 to 1000 µg/ml) were introduced to cultures of C. albicans. Following this, the survival fractions were examined to identify the MFC.

Microdilution method

The A3-M27 microdilution method was used to determine the minimum inhibitory concentration (MIC) of the substance. This method requires conducting the procedure under sterile conditions. Initially, 100 µl of RPMI1640 environment was added to each of the 96 sterile microplate wells.

Next, 100 microliters of 2000 ppm nanoparticles were added to the first microplate, resulting in a dilution of 1000 ppm in the initial wells. Then, 100 µl from the first wells were transferred to the second wells, and this process was repeated successively until reaching the last wells, resulting in dilutions of 1000, 500, 250, 125, 62.5, and 31.25 ppm, respectively.

To establish controls, positive and negative controls were included by adding 10 µl of fungal suspensions to all the wells. The microplates were subsequently incubated at 37 °C for 24 hours. After the incubation period, the wells were evaluated for turbidity, and the MFC was determined and reported.

AgNPs Characterization

The UV-visible spectra were obtained at room temperature using an Optizen 3220 UV spectrophotometer (Corea), with wavelengths of 300-600 nm and a step size of 2 nm. Fourier transform infrared (FT-IR) analysis was conducted using a Bruker FTIR alpha model. X-ray diffraction (XRD) patterns were analyzed using a X-ray diffractometer equipped with Ni-filtered Cu Kα radiation (Philips-X'pertpro). Scanning electron microscopy (SEM) was performed using a LEO instrument model 1455VP to examine the morphology of the synthesized nanoparticles (NPs). Particle size determination was conducted using a Vasco nanosizer (Cordouan, France). pH measurements were carried out using an 827 lab pH meter from Metrohm Company. The optical density, as determined by the MTT assay, was measured at 420 nm by a BioTeks Elx 800 microplate reader.

Computational method

To investigate the computational aspects, the crystal structures of bacteria were obtained from the Protein Data Bank (PDB) (www.rcsb.org). The Amber force field was chosen to minimize the docking process. Molecular docking experiments were conducted using MOE. The parameters of grid box were defined with center coordinates of 38.7238 in the x-direction, 10.2381 in the y-direction, and 25.6582 in the z-direction. The binding energy of the docking process was determined by employing the low RMSD evaluation method along with the Lamarckian genetic algorithm and the Amber 10H force field. Finally, the results were visually presented by Discovery Studio (2.1.0) [28]

Statistical analysis

Statistical significance among groups was evaluated using Student's t-test and analysis of variances. The data are presented as mean ± SD. A probability level of $p < 0.05$ was considered statistically significant.

RESULTS AND DISCUSSION

Ag Nanostructures Characterization

In general, the FT-IR spectrum is used to provide information about the structures and functional groups present in substances and the nature of molecular bonds. In this study, FTIR spectroscopy was applied to identify the functional groups involved in the bioreduction and capping of noble ions (Ag^+ to Ag^0). Fig. 1 illustrates the FTIR spectra of the synthesized silver nanoparticles (AgNPs) in the herbal extract.

The spectrum exhibited bands at 3445, 1653, 1457, and 750 cm−1. The broad peak in the range of 3307-3325 cm−1 indicates the presence of phenolic and flavonoid mixtures, which are responsible for the OH stretching. However, the AgNPs synthesized by using the extract show the same band at a higher frequency.

The sharp absorption peak observed at 1653 cm^{-1} can be attributed to the amide-I bond, indicating the involvement of proteins interacting with the green-synthesized AgNPs. The secondary structure of the proteins remains unaffected during or after the reaction with Ag^+ ions. The strong binding ability between the amino acid residues (carbonyl functional group) and the metal (capping agent) prevents agglomeration and provides medium stability [30]. The peak at 750 cm−1 indicates the presence of heterocyclic compounds

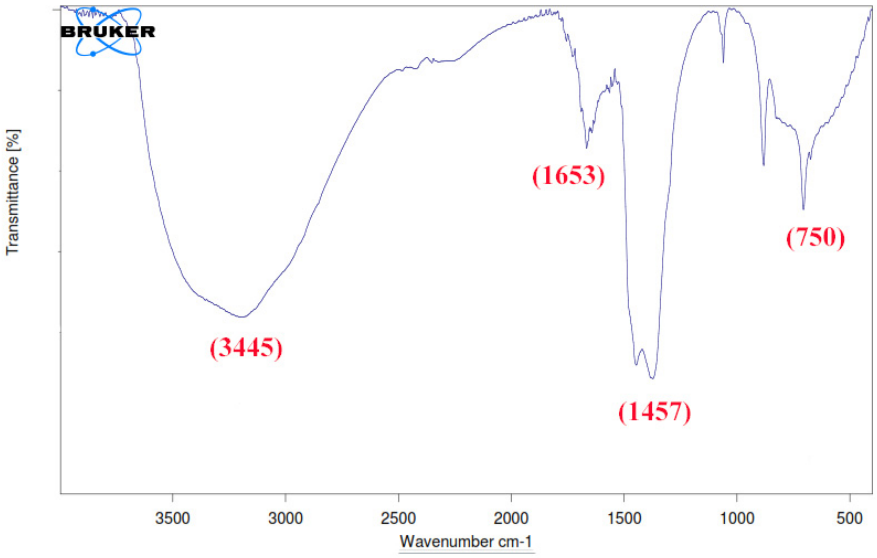

Fig.1. FT-IR spectrum of green synthesized Ag nanostructures.

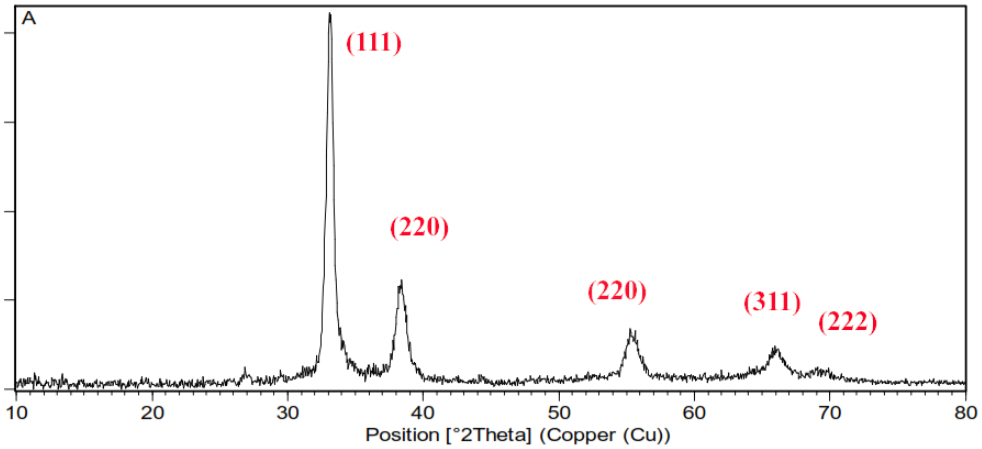

Fig. 2. X-ray diffraction pattern of green synthesized Ag nanostructures.

related to flavonoids [31]. The crystal structure of the synthesized AgNPs was analyzed using XRD technique. Multiple strong peaks were identified at (111), (220), (311), and (222) planes of the FCC lattice, indicating the crystal structure of Ag metal.

[32] (Fig. 2). These peaks are consistent with the standard Ag^0 pattern (JCPDS Card no. 04-0783) [33]. The (111) plane was found to be the dominant plane among the Ag planes. The average crystallite size (D) was determined by analyzing the (111) peak in the XRD patterns using the Scherrer Equation [34]: $D = k\lambda/B\cos\theta$. In this equation, B represents the full-width at half maximum (FWHM) of a diffraction peak; k stands for the Scherrer constant (0.89), and θ denotes the Bragg's angle. By applying this equation, the calculated crystal size from the XRD reflections was approximately 40±2 nm. The XRD lines reveal the presence of a smaller nanocrystalline phase within the nanosize range, as indicated by sharper reflexes with enhanced intensity.

The SEM images in Fig. 3(A, B) indicate the synthesized AgNPs at two magnifications. The SEM image clearly demonstrates that the AgNPs are spherical in shape and not agglomerated, with a diameter ranging from 40 to 50 nm [18].

The synthesis of the nanoparticles involves the participation of biomolecules from the extract, such as proteins, enzymes, terpenoids, and flavonoids cofactors, which play both a capping and reducing

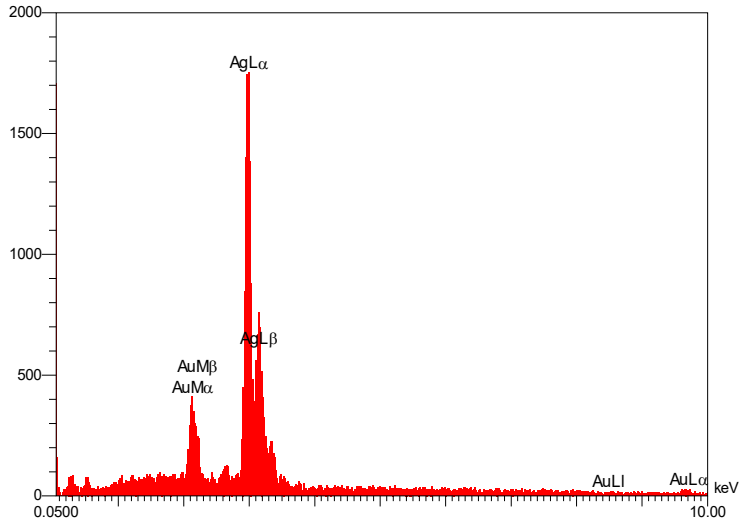

Fig.3. Scanning electron microscopy (SEM) of AgNPs synthesized in the presence of *Artemisia herba-alba* extract at two magnification and nanosizer curve (C).

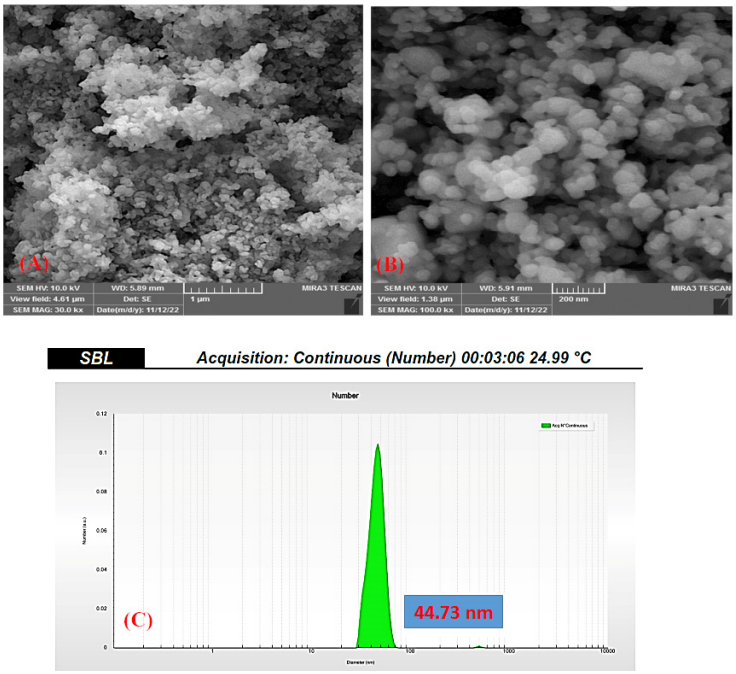

Fig.4. EDX image of synthesized Ag nanostructures

role. Additionally, due to the strong binding ability of amino acid residues (carbonyl group) with the metal capping agent, agglomeration behavior is prevented, ensuring medium stability [30].

To determine the actual size of nanoparticles more accurately, a nanosizer was utilized, and the particle size was analyzed using Statistical Bin Limits (SBL) analysis. The purpose was to reduce the error caused by agglomeration and obtain the true particle size by excluding the hydrodynamic radius. Fig. 3C presents the histogram of the nanosizer SBL analysis, which shows that the mean particle diameter is approximately 44 nm.

The results indicate a narrow size distribution and homogeneous dispersity of the nanoparticles. Additionally, Fig. 4 shows the results of the

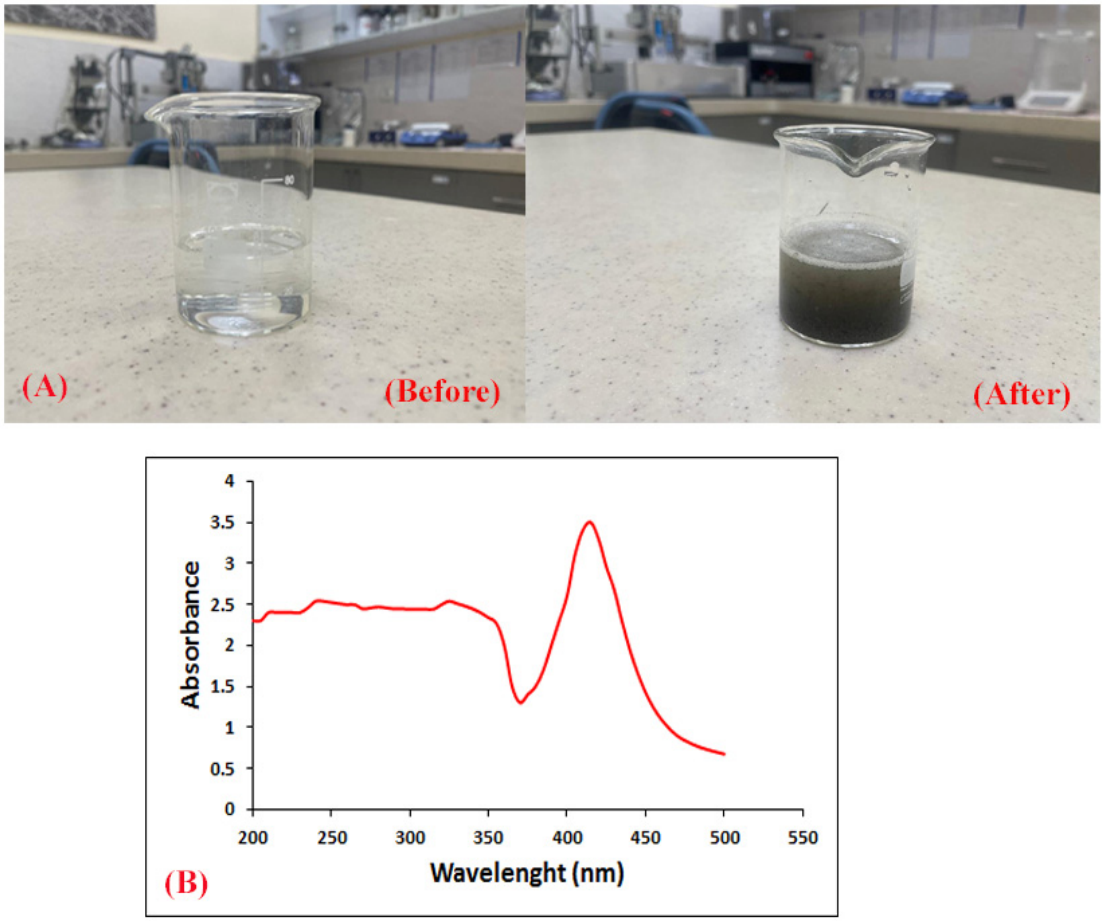

Fig.5. Photographic image of reduction of Ag^{+} to Ag^{0} before and after addition of herbal extract (A), UV–VIS spectra of silver nanoparticles in the presence of *Artemisia herba-alba extract* (B).

Energy Dispersive X-ray (EDX) analysis of the Ag nanoparticles. The examination of AgNPs using an EDX spectrometer confirms the presence of elemental signals corresponding to silver and demonstrates a uniform distribution of AgNPs.

The prominent peak of silver in the spectrum strongly indicates the reduction of $AgNO_3$ to AgNPs. The vertical axis represents the number of X-ray counts, whereas the horizontal axis denotes energy in KeV. The detection lines for the primary emission energy of silver are clearly identified, and they correspond to the peaks observed in the spectrum, providing confirmation that silver has been accurately detected and is present in the solution.

Ag nanoparticles synthesis investigation

When Artemisia extract was added to the AgNO3 solution at room temperature, the reaction mixture turned completely brown, as shown in Fig. 5A. This brown color corresponds to the surface plasmon resonance of silver nanoparticles formed within the reaction mixture.

UV-Vis spectroscopy is commonly used to detect the distribution and size of AgNPs by measuring the surface plasmon resonance (SPR) excitation [35]. As the size of the metal particles increases, the absorption band of SPR shifts towards higher wavelengths. Fig. 5B displays the UV-Vis spectra illustrating the silver nanoparticles (AgNPs) prepared under various pH levels in the presence of Artemisia.

The most prominent symmetric absorbance band is observed at around 420 nm and 415 nm (pH 8 and 10) and 395 nm (pH 12) in the UV-Vis spectra, indicating the formation of well-dispersed AgNPs. As the pH value rises, the absorption peak intensity increases steadily, and when the pH value

reaches 12, the band noticeably shifts towards lower wavelengths.

Metallic particles having small diameters exhibit high optical absorbance due to distinct electronic energy levels. Higher pH values promote alkaline hydrolysis, leading to the production of smaller molecular fragments with higher reducibility and affinity, which are crucial for the synthesis of stable and well-dispersed AgNPs. Furthermore, the concentration of silver salt and the volume of the extract are additional factors that can significantly influence the shape of silver nanoparticles.

Figs. 6A, 6B, and 6C illustrate the UV-Vis spectra of AgNPs prepared using different concentrations of $AgNO_3$, volumes of herbal extract, and synthesis reaction temperatures, respectively. An increase in the metallic precursor content results in a higher strength of the absorption peak, while a

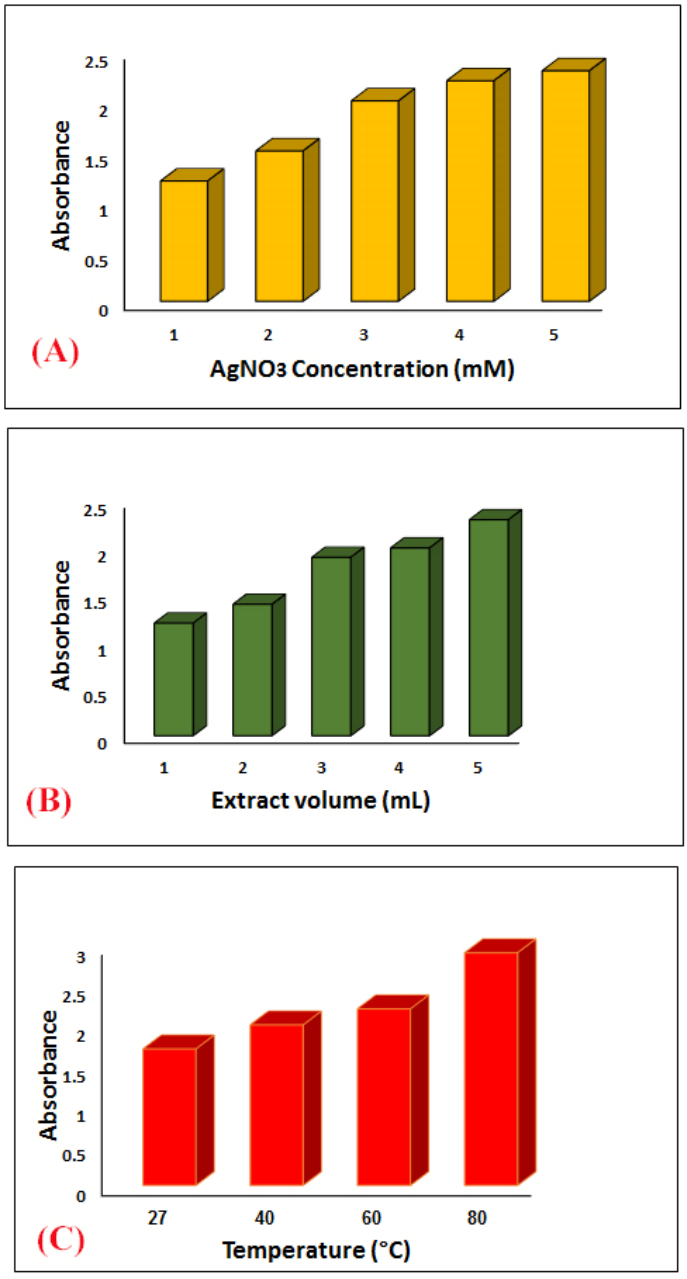

Fig.6. Various $AgNO_3$ concentration effect (A) extract volume (B) and temperature (C) on production of AgNPs using various aqueous extracts respectively.

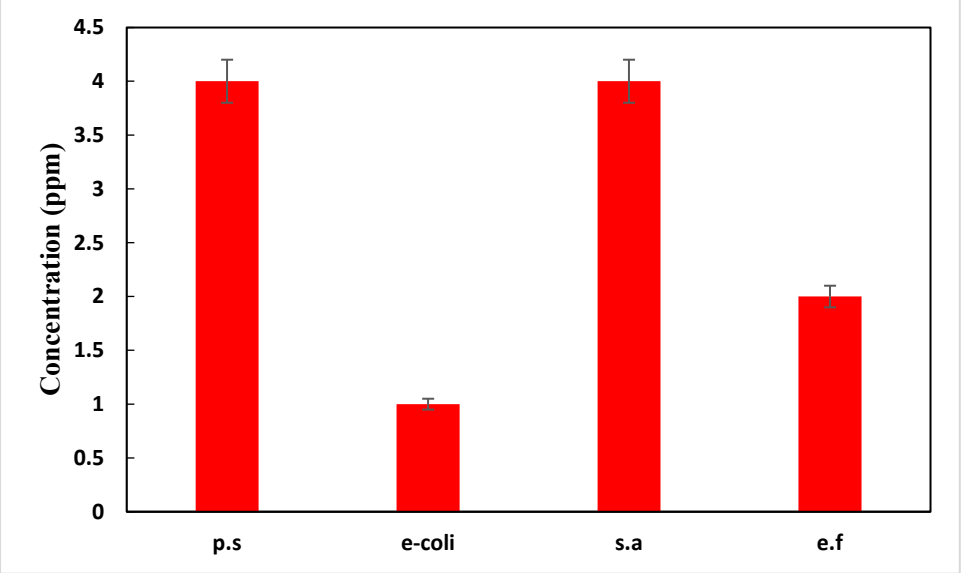

Fig.7. Mortality (%) of the green synthesized silver nanoparticles on various bacteria.

displacement towards longer wavelengths is seen in the UV-Vis spectrum absorption of nanoparticles synthesized with higher content of metallic precursor (s not shown).

The results indicate that elevating the AgNO3 concentration enhances the peak intensity for all samples. Additionally, the effect of varying temperature on the synthesis of AgNPs in the presence of the extract was investigated (Fig. 6C), revealing that an increase in temperature did not result in a reduction in absorption peaks. These findings suggest a better synthesis efficiency even at higher temperatures.

Evaluation of antimicrobial properties of Ag nanoparticles

Antibiotic resistance has become a major public health concern in recent times. This resistance is closely linked to oxidative stress, which contributes to the emergence of resistant bacterial strains. The antimicrobial efficacy of the green-synthesized AgNPs was investigated against three gram-positive and four gram-negative bacteria, including B. subtilis, M. luteus, S. aureus, K. pneumonia, E. coli, P. mirabilis, P. aeruginosa, respectively.

The bactericidal characteristics of AgNPs depend on their stability within the growth medium, the presence of capping agents, and the shape/size of the nanoparticles, which play a crucial role in enhancing their antimicrobial properties [36]. In general, the smaller size and higher surface-to-volume ratio of AgNPs contribute to their enhanced antimicrobial activity by allowing active silver atoms to be present on their surface [37].

The obtained results revealed varying antimicrobial activity among the different bacterial strains. Both gram-positive and gram-negative bacteria showed sensitivity to the tested samples. The MIC50 values for the synthesized nanoparticles were 8, 4, 4, 2, 2, 1, and 4 ppm for the respective strains, as depicted in Fig. 7.

While there is a noticeable difference in the activities of AgNPs against the seven bacterial strains, the antimicrobial activity against B. subtilis is particularly higher in comparison with the others.

The interaction of silver particles with thiol group compounds, present in the respiratory enzymes of bacterial cells, is responsible for their effectiveness against bacteria. Silver binds to the bacterial cell wall and membrane, hindering the respiratory process. Due to their larger surface area, AgNPs exhibit increased antimicrobial activity by attaching to the bacterial cell membrane and penetrating the bacteria [38]. The bacterial membrane covers sulfur-containing proteins, and silver nanoparticles interact with these proteins within the cell, in addition to the phosphorus-containing compounds such as DNA. AgNPs preferably target the respiratory chain of bacteria.

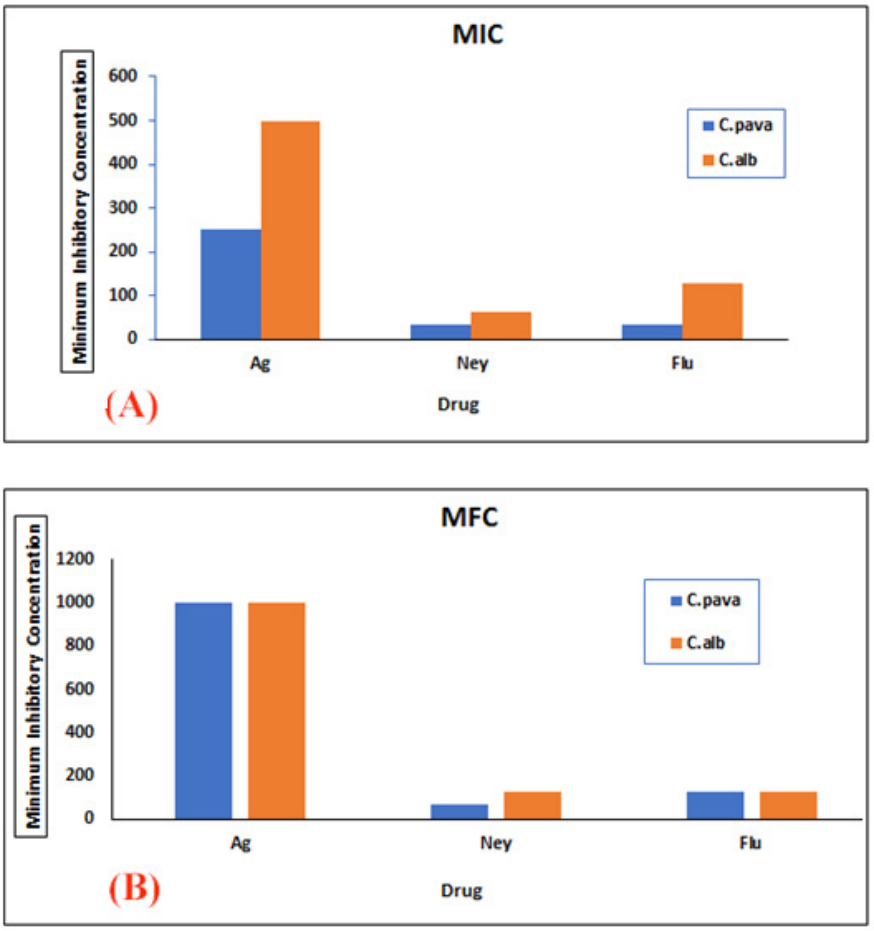

Fig.8. Mortality (%) of the green synthesized silver nanoparticles on various fungi

Antifungal characteristics of AgNps

Silver and silver compounds are recognized for their efficient application in burn and chronic wound treatments due to their antimicrobial properties. Although the mechanism of fungicidal activity of AgNps is still a subject of debate, they are acknowledged to be harmful to fungal cells [39]. The antifungal activity of AgNps, which is dependent on factors such as size, shape, and surface modification, can vary when prepared using different methods [40]. In this study, the antifungal activity of AgNps synthesized through green methods was examined against C. albicans, a common opportunistic fungal pathogen. The evaluation was conducted using broth microdilution and spot assays (Fig. 8). The broth microdilution assay demonstrated that AgNps exhibited growth inhibition of Candida at lower concentrations, with significant reduction observed at 5 µg/mL, while nearly complete inhibition occurred at 40 µg/mL (MIC for AgNps) (Fig. 8A and B). Additionally, the spot assay confirmed the results of the broth microdilution, showing that Candida cells exhibited lower sensitivity towards AgNps at 5 µg/mL and increased sensitivity at 40 µg/mL.

The antifungal activity of AgNps was evaluated by comparing the growth of cells with a control group (without AgNps). The enhanced antifungal efficacy of AgNps can be attributed to their high surface-to-volume ratio and the presence of {111} facets, which enable direct interaction with fungal cells in comparison to the bulk silver.

Understanding the intracellular pathways and unraveling the molecular and cellular mechanisms participating in the antifungal activity of AgNps is essential to ensure their safe utilization in medicine. Hence, we conducted a systematic investigation in the subsequent sections to explore the underlying molecular and cellular mechanisms participating

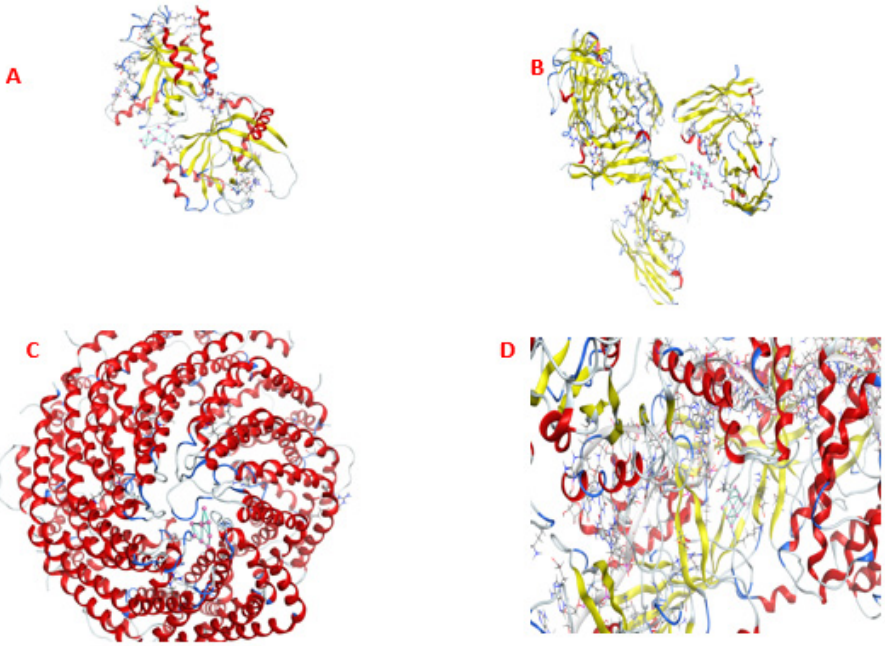

Fig. 9. Pose of binding of Ag with (A)Staphylococcus aureus (B) Escherichia coli(C) Pseudomonas aeruginosam (D) Streptococcus

in the antifungal activity of AgNps [41].

The antifungal activity was assessed by measuring the diameter of the growth inhibition zone surrounding the discs. A larger zone of inhibition indicates a stronger antifungal activity, with a MIC of 500. The Minimum Fungicidal Concentration (MFC), which represents the lowest concentration of Ag nanoparticles needed to impact the viability of C. albicans, was determined through MFC measurement. C. albicans cultures were exposed to varying concentrations of nanoparticles (62.5-1000 µg/mL), and the survival fractions were examined. It was observed that the cell counts of C. albicans decreased with increasing nanoparticle concentration. To achieve >90% fungicidal activity, a minimum concentration of 500 µg/mL was required, with a MIC of 250 for c.para.

Docking study of Ag nanoparticles

The Protein Data Bank (PDB) (www.rcsb.org) was utilized to obtain crystal structures of bacteria, which were prepared for the study. The Amber force field was selected to minimize the docking process. To perform the molecular docking experiment, AutoDock4 [42]. was employed.

The hydrophobic nature of proteins, amino acids, and bacterial structures contributes to their ability to repel water in biochemical systems. This effect is attributed to hydrogen bonding within their structures[43]. Fig. 9 (A-D) depicts the active and binding sites of Ag with various bacteria. To assess and predict the binding affinity between the ligands and target proteins, the binding free energies (ΔG) were calculated for both the docking models and the crystal structures. This analysis was conducted to evaluate the accuracy of the binding ability. A lower value of binding energy indicates a stronger binding strength between ligands and the docking model. To evaluate the strength of the binding between Ag and bacteria, the Ag-bacteria docked complexes were analyzed by considering the minimum binding energy values and the interaction patterns of Ag (hydrogen/ hydrophobic). The docking results, as presented in Table 1, revealed that AgNPs exhibited favorable interactions with bacteria, demonstrating their antibacterial activity in a solvent environment. Among the bacteria tested, E. coli displayed the lowest binding energy, indicating a strong interaction between Ag and E. coli.

The reversible binding or interaction of ligands with biological macromolecules is a fundamental process that influences various aspects of biochemistry and cell biology [44] . In biochemistry, binding events are rarely isolated occurrences; instead, they are often interconnected with other reactions, including protonation changes, interactions with other

Table 1. Docking energy values ΔG in kcal/mol of Ag interaction with bacteria

Compound	Docking Energy kcal/mol
Staphylococcus aureus	-6.78
Escherichia coli	-7.89
Pseudomonas aeruginosa	-5.34
Streptococcus	-6.48

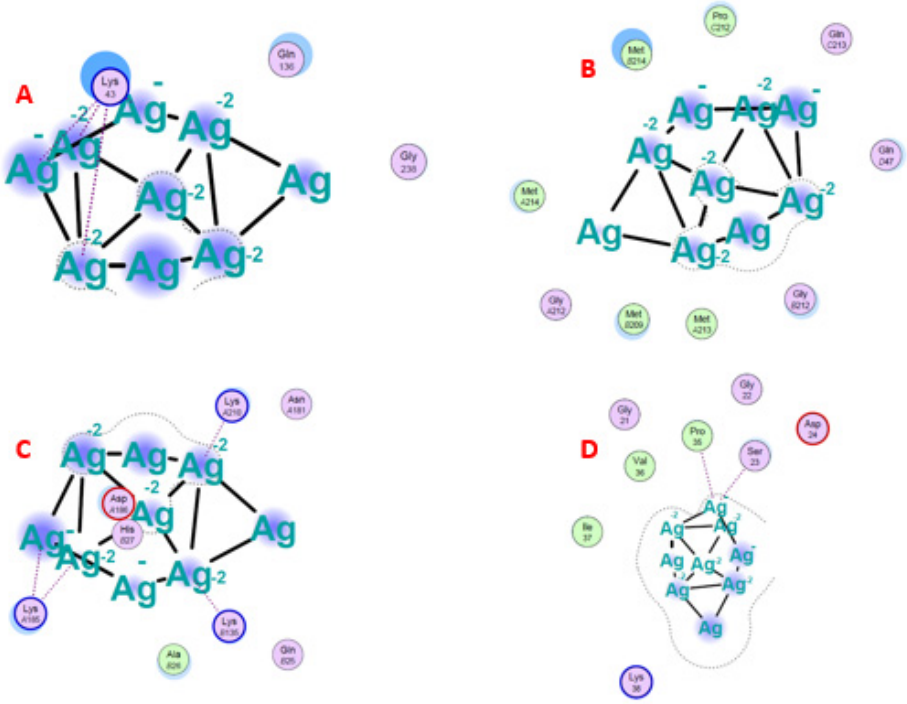

Fig. 10. Acid amine interaction in (A) Escherichia coli with Ag, (B) Pseudomonas aeruginosa with Ag, (C) Staphylococcus aureus with Ag and (D) Streptococcus with Ag.

ligands, structural transitions, and folding processes. Merely stating that something binds is often insufficient. A comprehensive understanding of binding entails assessing, stoichiometry, affinity and the interconnectedness of linked reactions. Molecular binding takes place within biological complexes, such as interactions between protein pairs or sets, as well as between a protein and the small molecule ligand it binds. Binding also occurs within biological chemical systems. Molecular binding can be classified into distinct categories: non-covalent binding, characterized by the absence of chemical bonds between the interacting molecules, thus enabling fully reversible associations. Conversely, reversible covalent binding involves the establishment of a chemical bond. Nevertheless, the free energy difference between the reactants noncovalently bonded and the product in the bonded state is close to equilibrium, and the activation barrier for the reverse reaction, leading to the cleavage of the chemical bond, is relatively low. This facilitates the facile reversal of the binding process. Irreversible covalent binding involves the formation of a chemical bond in which the product is significantly more thermodynamically stable than the reactants, making the reverse reaction highly unlikely. Fig. 10 (A-D) depicts the amino acids that interact with Ag in bacterial structures. In E. coli, Ag exhibits interactions with Gln, Lys, and Gly. Pseudomonas aeruginosa shows interactions with Met, Pro, Gly, and Gln. Staphylococcus aureus demonstrates interactions with Lys, Asn, Asp, His, Gln, and Aln, while Streptococcus displays interactions with Gly, Pro, Ser, Val, Asp, Ile, and Lys.

CONCLUSION

The present study demonstrates the preparation of silver nanoparticles (AgNPs) using herbal extracts. This method is simple, inexpensive, environmentally friendly, and reliable, making it a recommended approach for industrial production of metal nanoparticles without the use of hazardous reducing and capping agents.

The synthesized AgNPs were analyzed using SEM and XRD, revealing spherical nanoparticles with a nanoscale diameter of approximately 44 nm in the presence of Amygdalus lycioides. The optimal concentrations of the participating compounds and reaction time were determined to synthesize stable silver nanoparticles. The antifungal activity of the nanoparticles was observed, inhibiting the formation of blood clots.

Moreover, considering the antimicrobial properties and stability of these nanoparticles, it is evident that they hold potential for various biomedical applications, including cosmetics. The binding energy and activation properties of the nanoparticles is in very good agreement with experimental data.

ACKNOWLEDGMENT

This article is the result of a research project approved by the Kerman University of Medical Sciences, No# 98000427 which has been done with the financial support of the Deputy for Research and Technology of this university.

COMPETING INTERESTS

There is no conflict of interests in the manuscript.

REFERENCES

1. Beg M, Maji A, Mandal AK, Das S, Aktara MN, Jha PK, et al. Green synthesis of silver nanoparticles using Pongamia pinnata seed: Characterization, antibacterial property, and spectroscopic investigation of interaction with human serum albumin. Journal of Molecular Recognition. 2017;30(1):e2565.
2. Jiang K, Pinchuk AO. Chapter Two - Noble Metal Nanomaterials: Synthetic Routes, Fundamental Properties, and Promising Applications. In: Camley RE, Stamps RL, editors. Solid State Physics. 66: Academic Press; 2015. p. 131-211.
3. Salimi K, Eghbali S, Jasemi A, Shokrani Foroushani R, Joneidi Yekta H, Latifi M, et al. An Artificial Soft Tissue Made of Nano-Alginate Polymer Using Bioxfab 3D Bioprinter for Treatment of Injuries. Nanochemistry Research. 2020;5(2):120-7.
4. Baneshi N, Moghadas BK, Adetunla A, Yusof MYPM, Dehghani M, Khandan A, et al. Investigation the mechanical properties of a novel multicomponent scaffold coated with a new bio-nanocomposite for bone tissue engineering: Fabrication, simulation and characterization. Journal of Materials Research and Technology. 2021;15:5526-39.
5. Solomon MM, Umoren SA. In-situ preparation, characterization and anticorrosion property of polypropylene glycol/silver nanoparticles composite for mild steel corrosion in acid solution. Journal of Colloid and Interface Science. 2016;462:29-41.
6. Ishiwatari S, Suzuki T, Hitomi T, Yoshino T, Matsukuma S, Tsuji T. Effects of methyl paraben on skin keratinocytes. Journal of Applied Toxicology. 2007;27(1):1-9.
7. Silver S, Phung LT, Silver G. Silver as biocides in burn and wound dressings and bacterial resistance to silver compounds. Journal of Industrial Microbiology and Biotechnology. 2006;33(7):627-34.
8. Liang H, Mirinejad MS, Asefnejad A, Baharifar H, Li X, Saber-Samandari S, et al. Fabrication of tragacanthin gum-carboxymethyl chitosan bio-nanocomposite wound dressing with silver-titanium nanoparticles using freeze-drying method. Materials Chemistry and Physics. 2022;279:125770.
9. Bastús NG, Merkoçi F, Piella J, Puntes V. Synthesis of Highly Monodisperse Citrate-Stabilized Silver Nanoparticles of up to 200 nm: Kinetic Control and Catalytic Properties. Chemistry of Materials. 2014;26(9):2836-46.
10. Bahadur NM, Furusawa T, Sato M, Kurayama F, Siddiquey IA, Suzuki N. Fast and facile synthesis of silica coated silver nanoparticles by microwave irradiation. Journal of Colloid and Interface Science. 2011;355(2):312-20.
11. Kshirsagar P, Sangaru SS, Malvindi MA, Martiradonna L, Cingolani R, Pompa PP. Synthesis of highly stable silver nanoparticles by photoreduction and their size fractionation by phase transfer method. Colloids and Surfaces A: Physicochemical and Engineering Aspects. 2011;392(1):264-70.
12. Daengsakul S, Mongkolkachit C, Thomas C, Siri S, Thomas I, Amornkitbamrung V, et al. A simple thermal decomposition synthesis, magnetic properties, and cytotoxicity of $La_{0.7}Sr_{0.3}MnO_3$ nanoparticles. Applied Physics A. 2009;96(3):691-9.
13. Naghdi M, Taheran M, Brar SK, Verma M, Surampalli RY, Valero JR. Green and energy-efficient methods for the production of metallic nanoparticles. Beilstein Journal of Nanotechnology. 2015;6:2354-76.
14. Usha Rani P, Rajasekharreddy P. Green synthesis of silver-protein (core–shell) nanoparticles using Piper betle L. leaf extract and its ecotoxicological studies on Daphnia magna. Colloids and Surfaces A: Physicochemical and Engineering Aspects. 2011;389(1):188-94.
15. Amiri M, Salavati-Niasari M, Akbari A, Gholami T. Removal of malachite green (a toxic dye) from water by cobalt ferrite silica magnetic nanocomposite: Herbal and green sol-gel autocombustion synthesis. International Journal of Hydrogen Energy. 2017;42(39):24846-60.
16. Amiri M, Pardakhti A, Ahmadi-Zeidabadi M, Akbari A, Salavati-Niasari M. Magnetic nickel ferrite nanoparticles: Green synthesis by Urtica and therapeutic effect of frequency magnetic field on creating cytotoxic response in neural cell lines. Colloids and Surfaces B: Biointerfaces. 2018;172:244-53.
17. Amiri M, Salavati-Niasari M, Pardakhty A, Ahmadi M, Akbari A. Caffeine: A novel green precursor for synthesis

of magnetic $CoFe_2O_4$ nanoparticles and pH-sensitive magnetic alginate beads for drug delivery. Materials Science and Engineering: C. 2017;76:1085-93.
18. Raja S, Ramesh V, Thivaharan V. Green biosynthesis of silver nanoparticles using Calliandra haematocephala leaf extract, their antibacterial activity and hydrogen peroxide sensing capability. Arabian Journal of Chemistry. 2017;10(2):253-61.
19. Kumar Sur U, Ankamwar B, Karmakar S, Halder A, Das P. Green synthesis of Silver nanoparticles using the plant extract of Shikakai and Reetha. Materials Today: Proceedings. 2018;5(1, Part 2):2321-9.
20. Majeed S, Abdullah MSb, Nanda A, Ansari MT. In vitro study of the antibacterial and anticancer activities of silver nanoparticles synthesized from Penicillium brevicompactum (MTCC-1999). Journal of Taibah University for Science. 2016;10(4):614-20.
21. Babu SA, Prabu HG. Synthesis of AgNPs using the extract of Calotropis procera flower at room temperature. Materials Letters. 2011;65(11):1675-7.
22. Surya S, Kumar GD, Rajakumar R, editors. Green Synthesis of Silver Nanoparticles from Flower Extract of Hibiscus rosa-sinensis and Its Antibacterial Activity2016.
23. Valli G, Suganya M. Biogenic synthesis of copper nanoparticles using Delonix elata flower extract.7(5):776–9.
24. Lee SH, Jun B-H. Silver Nanoparticles: Synthesis and Application for Nanomedicine. International Journal of Molecular Sciences [Internet]. 2019; 20(4).
25. Maryan AS, Montazer M, Harifi T. One step synthesis of silver nanoparticles and discoloration of blue cotton denim garment in alkali media. Journal of Polymer Research. 2013;20(8):189.
26. Elshikh M, Ahmed S, Funston S, Dunlop P, McGaw M, Marchant R, et al. Resazurin-based 96-well plate microdilution method for the determination of minimum inhibitory concentration of biosurfactants. Biotechnology Letters. 2016;38(6):1015-9.
27. Eslaminejad T, Nematollahi-Mahani SN, Ansari M. Cationic β-Cyclodextrin–Chitosan Conjugates as Potential Carrier for pmCherry-C1 Gene Delivery. Molecular Biotechnology. 2016;58(4):287-98.
28. San Diego C. Accelrys Software, Disovery Studio, Version 4.1. Accelrys Software Inc 2007.
29. Isaac RSR, Sakthivel G, Murthy C. Green Synthesis of Gold and Silver Nanoparticles Using Averrhoa bilimbi Fruit Extract. Journal of Nanotechnology. 2013;2013:906592.
30. Boopathi S, Gopinath S, Boopathi T, Balamurugan V, Rajeshkumar R, Sundararaman M. Characterization and Antimicrobial Properties of Silver and Silver Oxide Nanoparticles Synthesized by Cell-Free Extract of a Mangrove-Associated Pseudomonas aeruginosa M6 Using Two Different Thermal Treatments. Industrial & Engineering Chemistry Research. 2012;51(17):5976-85.
31. Kačuráková M, Capek P, Sasinková V, Wellner N, Ebringerová A. FT-IR study of plant cell wall model compounds: pectic polysaccharides and hemicelluloses. Carbohydrate Polymers. 2000;43(2):195-203.
32. Gogoi N, Babu PJ, Mahanta C, Bora U. Green synthesis and characterization of silver nanoparticles using alcoholic flower extract of Nyctanthes arbortristis and in vitro investigation of their antibacterial and cytotoxic activities. Materials Science and Engineering: C. 2015;46:463-9.
33. Coseri S, Spatareanu A, Sacarescu L, Rimbu C, Suteu D, Spirk S, et al. Green synthesis of the silver nanoparticles mediated by pullulan and 6-carboxypullulan. Carbohydrate Polymers. 2015;116:9-17.
34. Amiri M, Salavati-Niasari M, Akbari A, Razavi R. Sol–gel auto-combustion synthesize and characterization of a novel anticorrosive cobalt ferrite nanoparticles dispersed in silica matrix. Journal of Materials Science: Materials in Electronics. 2017;28(14):10495-508.
35. Lee KY, Mooney DJ. Alginate: Properties and biomedical applications. Progress in Polymer Science. 2012;37(1):106-26.
36. Pal S, Tak Yu K, Song Joon M. Does the Antibacterial Activity of Silver Nanoparticles Depend on the Shape of the Nanoparticle? A Study of the Gram-Negative Bacterium Escherichia coli. Applied and Environmental Microbiology. 2007;73(6):1712-20.
37. Ocsoy I, Demirbas A, McLamore ES, Altinsoy B, Ildiz N, Baldemir A. Green synthesis with incorporated hydrothermal approaches for silver nanoparticles formation and enhanced antimicrobial activity against bacterial and fungal pathogens. Journal of Molecular Liquids. 2017;238:263-9.
38. Rai M, Yadav A, Gade A. Silver nanoparticles as a new generation of antimicrobials. Biotechnology Advances. 2009;27(1):76-83.
39. Singh R, Wagh P, Wadhwani S, Gaidhani S, Kumbhar A, Bellare J, et al. Synthesis, optimization, and characterization of silver nanoparticles from Acinetobacter calcoaceticus and their enhanced antibacterial activity when combined with antibiotics. International Journal of Nanomedicine. 2013;8(null):4277-90.
40. Singh P, Kim YJ, Singh H, Wang C, Hwang KH, Farh ME-A, et al. Biosynthesis, characterization, and antimicrobial applications of silver nanoparticles. International Journal of Nanomedicine. 2015;10(null):2567-77.
41. Morones JR, Elechiguerra JL, Camacho A, Holt K, Kouri JB, Ramírez JT, et al. The bactericidal effect of silver nanoparticles. Nanotechnology. 2005;16(10):2346.
42. Morris GM, Huey R, Lindstrom W, Sanner MF, Belew RK, Goodsell DS, et al. AutoDock4 and AutoDockTools4: Automated docking with selective receptor flexibility. Journal of computational chemistry. 2009;30(16):2785-91.
43. Lillehoj EP, Malik VS, editors. Protein purification. Bioprocesses and Engineering; 1989 1989//; Berlin, Heidelberg: Springer Berlin Heidelberg.
44. Shriver JW, Edmondson SP. Ligand-Binding Interactions and Stability. In: Shriver JW, editor. Protein Structure, Stability, and Interactions. Totowa, NJ: Humana Press; 2009. p. 135-64.